In-Situ Study Of The Low Overpotential "Dimer Pathway" For Electrocatalytic Carbon Dioxide Reduction By Manganese Carbonyl Complexes

Gaia Neri,[1] Paul M. Donaldson[2] and Alexander J. Cowan[1,*]

1. Department of Chemistry and Stephenson Institute for Renewable Energy, University of Liverpool, L69 7ZD, Liverpool, UK,

2. Central Laser Facility, STFC Rutherford Appleton Laboratory, Harwell, Didcot, Oxfordshire, OX11 0QX, UK

*acowan@liverpool.ac.uk

ABSTRACT

The electrocatalytic reduction of CO_2 using [*fac*-Mn(bpy)$(CO)_3$Br] (bpy = 2,2'- bipyridine) and its derivatives has been the subject of numerous recent studies. However the mechanisms of catalysis are still debated. Here we carry out in-situ vibrational sum-frequency generation (VSFG) spectroelectrochemistry to examine how this catalyst behaves at an electrode surface. In particular, a low overpotential pathway involving a dimeric manganese has been reported in several studies using substituted bipyridine ligands. Here, we find that the "dimer pathway" can also occur with the unsubsituted bipyridine complexes. Specifically we can observe spectroscopic evidence of the interaction between [Mn_2(bpy)$_2(CO)_6$] with CO_2 in the presence of a suitable acid. Detailed VSFG studies of [Mn_2(bpy)$_2(CO)_6$], including of the potential dependence of the surface ν(CO) mode, allow us to construct a model of how it accumulates and behaves at the electrode surface under potentiostatic control.

INTRODUCTION

CO_2 is typically considered a waste molecule, however if effective electrocatalytic materials or molecules for the reduction of CO_2 can be developed it would instead be a useful feedstock from which carbon fuels (e.g. CH_4, CH_3OH) and industrially important molecules (e.g. CO, HCO_2H) could be sustainably produced. Molecular electrocatalysts based on abundant metal centres such as Mn and Fe are receiving particular attention as they have been shown to be able to reduce CO_2 to CO ($CO_2 + 2e^- + 2H^+ \rightarrow CO$ E^0 = -0.53 V vs. NHE at pH 7)[1] with excellent selectivity, even in water,[2–5] conditions where H_2 evolution can effectively compete ($2H^+ + 2e^- \rightarrow H_2$ E^0 = -0.41 V vs. NHE at pH 7). Interest in Mn based molecular catalysts increased

greatly following the report by Deronzier et al. in 2011 that [*fac*-Mn(bpy)$(CO)_3$Br] (bpy = 2,2'- bipyridine) was a pre-catalyst for the reduction of CO_2 to CO in acetonitrile/water mixtures.[6] From here onwards the *fac* labelled is omitted and instead geometry labels are included solely for *mer*-complexes. Prior to this work the electrochemistry of [Mn(bpy)$(CO)_3$Br], and closely related complexes, had been studied in detail[7–9] in aprotic solvents but in contrast to analogous Re complexes[10] CO_2 reduction had not been reported. For Mn complexes the presence of water, or an alternative Brønsted acid, is vital to enabling CO_2 binding to the Mn centre.[11–13]

Significant advances have since been made, both in the synthesis of new Mn carbonyl catalysts with improved catalytic activity and in the understanding of the catalytic mechanisms occurring which are summarised in two recent comprehensive reviews.[14,15] It is known that the halide ligand can readily exchange with the solvent or acid molecules in solution giving rise to a mixture of $[Mn(bpy)(CO)_3X]^{n+}$ (X = Br^- n = 0; X = CH_3CN, H_2O, n = 1). Upon 1 e^- reduction these complexes readily undergo loss of the axial X ligand to form $[Mn(bpy)(CO)_3]^\bullet$, which in solution at room temperature is very short-lived and readily dimerizes to form $[Mn_2(bpy)_2(CO)_6]$,[16] see scheme 1. The dimer complex can then be further reduced to form 2 equivalents of $[Mn(bpy)(CO)_3]^-$. It is widely accepted that in most electrocatalytic studies the active catalyst is $[Mn(bpy)(CO)_3]^-$, or the relevant derivative of this complex. Detailed theory[11–13] and spectroscopic studies[14,17–20] have identified the presence of two catalytic pathways ("protonation first" and "reduction first") following the formation of $[Mn(bpy)(CO)_3(CO_2H)]$, with the balance of contribution from each depending on the applied potential and the acid strength used.

In studies with substituted bipyridine (R-bpy = 4,4'-R-2,2'-bipyridine, R = methyl,[21] ^{t}Bu[22]) complexes an increase in current density under CO_2 has also been observed at potentials positive of where the reduction of the dimer complex occurs, indicating that CO_2 reduction does not solely proceed *via* the formation of $[Mn(R\text{-}bpy)(CO)_3]^-$. Pulsed-EPR spectroscopy of dimethyl bipyridine complexes in solution has shown that oxidative addition of CO_2 and H^+ to the dimer can also occur in solution (red pathway, scheme 1) leading to a third possible catalytic pathway where $[mer\text{-}Mn(bpy)(CO)_3(CO_2H)]^+$ is formed. Numerous studies, both with solution and heterogenized Mn catalysts, have since invoked the presence of this lower overpotential "dimer pathway" pathway.[21,23,24] However beyond the initial first study on $[Mn(Me_2\text{-}bpy)(CO)_3(CH_3CN)]$ the mechanism in solution has not been extensively examined and a 2nd explanation of the more positive onset potential for catalysis may also exist. Studies from Hartl et al.[7] demonstrated that at 200 K the related diimine complex, $[Mn(iPr\text{-}DAB)(CO)_3]^\bullet$ where iPr-DAB = 1,4-diisopropyl-1,4-diaza-1,3-butadiene, persists for long enough to undergo a reduction to directly form $[Mn(iPr\text{-}DAB)(CO)_3]^-$. $[Mn_2(iPr\text{-}DAB)_2(CO)_6]$ could still form in these studies but it was found to be *via* the reaction of $[Mn(iPr\text{-}DAB)(CO)_3]^\bullet$ with $[Mn(iPr\text{-}DAB)(CO)_3X]^{n+}$. Significantly the reduction of $[Mn(iPr\text{-}DAB)(CO)_3]^\bullet$ occurs at a potential positive of that required for the reduction of $[Mn(iPr\text{-}DAB)(CO)_3Br]$, enabling the formation of the catalytically active species $[Mn(iPr\text{-}DAB)(CO)_3]^-$ at a reduced overpotential. Such a pathway has also been proposed to be feasible at low temperature with [Mn(bpy)$(CO)_3$Br], (blue pathway in scheme 1).[7] Whilst dimerization has been prevented in room temperature solution through the use of bulky ligands[19,25] the potential role of the electrode surface in stabilizing $[Mn(bpy)(CO)_3]^\bullet$ at room temperature has not been explored. If even small concentrations of this

radical species could be stabilized on the surface for long enough to permit reduction to the catalytically active species $[Mn(bpy)(CO)_3]^-$ it would provide a further pathway for CO_2 reduction at lower overpotentials.

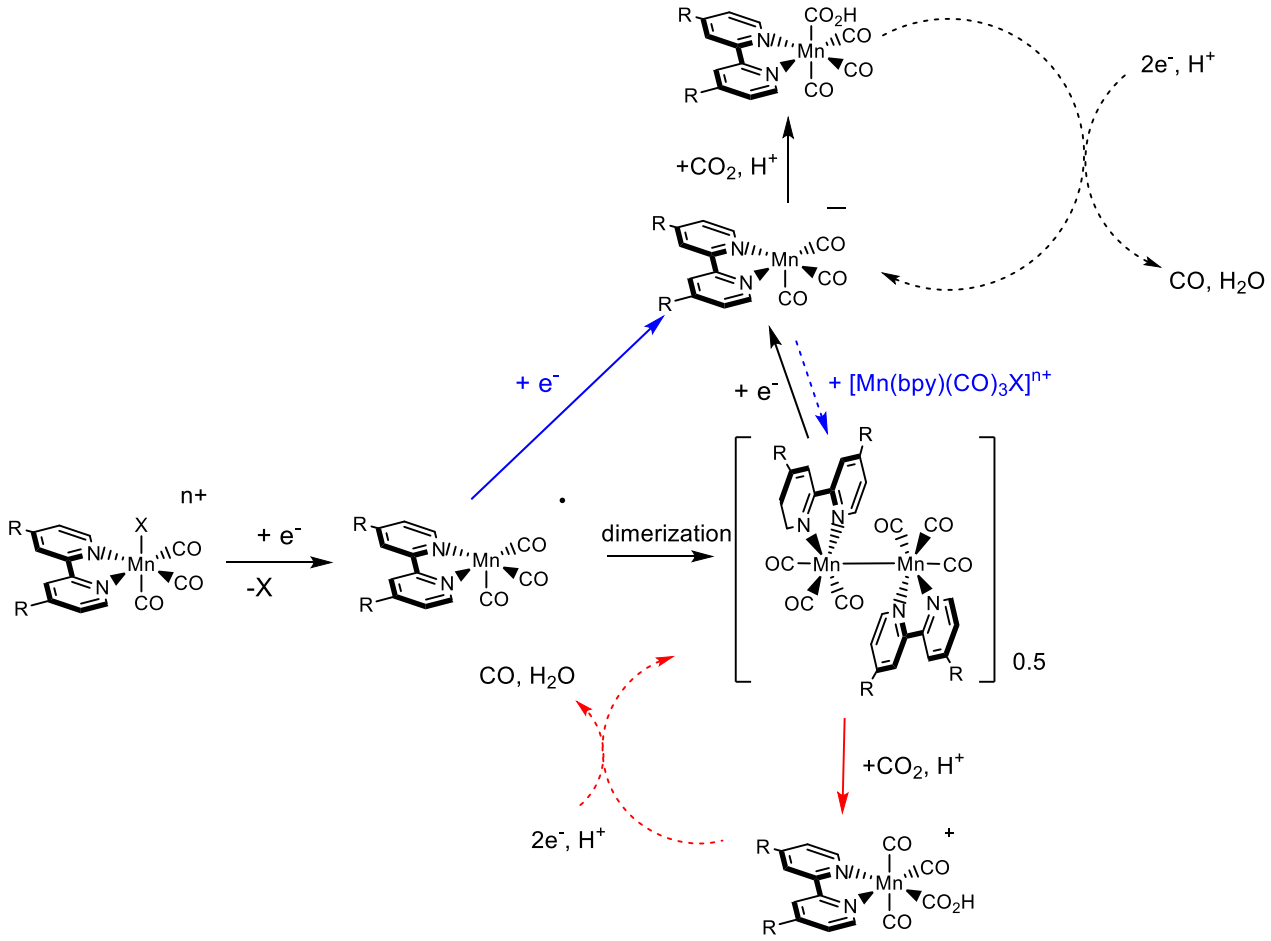

Scheme 1. *Proposed pathways for the electrocatalytic CO_2 reduction discussed using the complex $[Mn(R\text{-}bpy)(CO)_3X]^{n+}$. In this report we focus on the possible interaction of the dimeric complex with CO_2, H^+ (red arrows) and the possible formation of catalytic active complex $[Mn(bpy)(CO)_3]^-$ via a pathway previously proposed to occur at low temperature (blue arrows).*[8] *Dashed lines indicate that multiple steps are potentially occurring during the catalytic cycle.*

Detection of species at an electrode surface under potentiostatic control is challenging, as the presence of the complex in the bulk can mask weak spectral features. Vibrational Sum-Frequency Generation (VSFG) spectroscopy is inherently surface selective and it has been applied widely to the study of numerous electrode processes including electrocatalytic ethanol oxidation and carbon dioxide reduction amongst others.[26–28] Recently we used Spectro-electrochemical (SEC)-VSFG to monitor molecular electrocatalytic mechanisms for complexes that are not permanently (i.e. covalently) bound to the electrode surface.[20,29] In particular we have reported on the "protonation" first catalytic pathway that occurs following the reduction of $[Mn_2(bpy)_2(CO)_6]$ to $[Mn(bpy)(CO)_3]^-$ in the presence of CO_2.[20] Here we extend our study to explore the mechanisms of dimer formation and the role of a "dimer pathway" during catalysis.

METHODS

All chemicals (Bromopentacarbonylmanganese(i) (98%), 2,2-bipyridine (99%), acetonitrile (anhydrous, 99.8%), 2,2,2-TFE (≥99.5%), tetrabutylammonium hexafluorophosphate ($TBAPF_6$, ≥99.0%), phenol (≥99.0%), mercury (polarographic grade)) were purchased from Sigma and used without further purification, aside from ferrocene (≥98.0%), which was purified via sublimation and dried under vacuum. $[Mn(bpy)(CO)_3Br]$ was synthesised according to known procedures.[5]

A palmsens-3 potentiostat was used for all electrochemical experiments. The SEC cell for SFG experiments has been previously described,[20,24] briefly the main body is a Teflon cross piece (BOLA). The pseudo-reference electrode was a silver wire and the counter electrode was a Pt wire. The working electrode was a Au/Hg amalgam prepared by immersing a freshly polished polycrystalline gold disc electrode (0.031 cm^2 area, IJ cambria) in mercury for 1 min. The electrode was then left to dry for a minimum of 2 hours, before polishing using 15 and 6 μm diamond paste and finally 0.05 μm alumina slurry. Care was taken to avoid exposure to Au-Hg particles during this process. The electrode was sonicated for 30 s between each polish step. The electrode was secured in the cell via a screw fitting (BOLA) and separated from a CaF_2 window with a 50 μm Teflon spacer. For bulk electrochemical experiment, a pear-shaped flask was used. GCE and Au working electrodes were hand polished as described above. Ferrocene was added to the solution for bulk electrochemical experiments to reference the potential of the silver wire quasi-reference electrode. The UV-vis SEC experiments were carried out in a 2x1 cm custom-made quartz cell, using a platinum mesh as the working electrode, a silver wire quasi-reference electrode and a platinum mesh as the counter electrode, which was separated from the main cell compartment using a Vycor® double junction. The experiment was carried out by aligning the UV-vis light source on the working electrode and applying a constant potential (-1.05 $V_{Ag/Ag+}$) to the stirred solution to ensure complete electrolysis. A UV-vis absorbance spectrum of the solution (900 to 280 nm) was carried out every 2 or 5 minutes.

All SFG experiments were performed using the ULTRA B laser at the Central Laser Facility (STFC RAL), using a previously described set up.[20] Experiments were conducted with ppp polarisation (SFG, 800 nm, IR) and the IR and 800 nm beams were focussed at the electrode with spot sizes of ~200 and ~300 um and typical incident pulse energies were set to 2-3 μJ and < 1 μJ respectively (both at 10 kHz).

RESULTS

A. Linear-sweep voltammetry

The Linear Sweep Voltammograms (LSVs) of 1 mM $[Mn(bpy)(CO)_3Br]$ in acetonitrile under both Ar and CO_2 during VSFG experiments using an Au-Hg electrode are shown in figure 1a. Au-Hg electrodes are required for our SEC-VSFG studies as they provide: a suitably reflective surface for the spectroscopy, a large overpotential for H_2 evolution and reproducible VSFG responses with no observable breakdown of the complex under study. VSFG experiments with alternative metal electrodes such as Au have been attempted.

These were unsuccessful, as rapid fouling of the electrodes by surface bound CO occurs, suggesting that the low binding energy for CO on Hg surfaces may be an important factor.[30]

In the absence of an acid source the first two reductions in figure 1a at (-0.88 V (CO_2) and -0.90 V (Ar) both *vs*. an Ag pseudo reference electrode) and (-1.03 V (CO_2) and -1.04 V (Ar)) are assigned to $[Mn(bpy)(CO)_3(CH_3CN)]^+$ and $[Mn(bpy)(CO)_3Br]$ respectively.[14,31] A subsequent reduction (-1.26 V (CO_2), -1.22 V (Ar)) is due to the reduction of $[Mn_2(bpy)_2(CO)_6]$ which is known to form $[Mn(bpy)(CO)_3]^-$. In the presence of both trifluoroethanol (TFE) and phenol significant changes in the LSV are observed, figure 1b,c. Under Ar reductions at -0.88 V (both TFE and phenol) are present which are likely due to $[Mn(bpy)(CO)_3(CH_3CN)]^+$ and the lack of a feature assignable to $[Mn(bpy)(CO)_3Br]$ suggests that the presence of the acid facilitates ligand exchange, figures 1b,c. Between -0.9 and -1.1 V we observe a substantial increase in current under CO_2 when TFE or phenol are present (i_{cat}/i_p ~6.3, where i_{cat} and i_p are the maximum catalytic current (at potentials ≥ -1.1 V) and the current at the peak of the first reduction wave respectively). LSV's under Ar show that between -0.9 and -1.1 V $[Mn_2(bpy)_2(CO)_6]$ is expected to be present as it is not reduced to form $[Mn(bpy)(CO)_3]^-$ until -1.23 V, figure 1b. We also see similar levels of current enhancement under CO_2 with phenol and TFE as acid sources using a glassy carbon electrode (GCE) or an Au electrode indicating that the behaviour is not specific to Au-Hg, figures S1-3. Electrocatalytic CO_2 reduction in the potential region where the dimer complex is present has been reported multiple times[21,23,24,32] for complexes with 4,4'-substituted bipyridine ligands but catalysis by this lower overpotential pathway is not widely reported using the prototypical complex, $[Mn(bpy)(CO)_3X]^{n+}$, in solution. However these results indicate that in the presence of a suitable acid source it can occur.

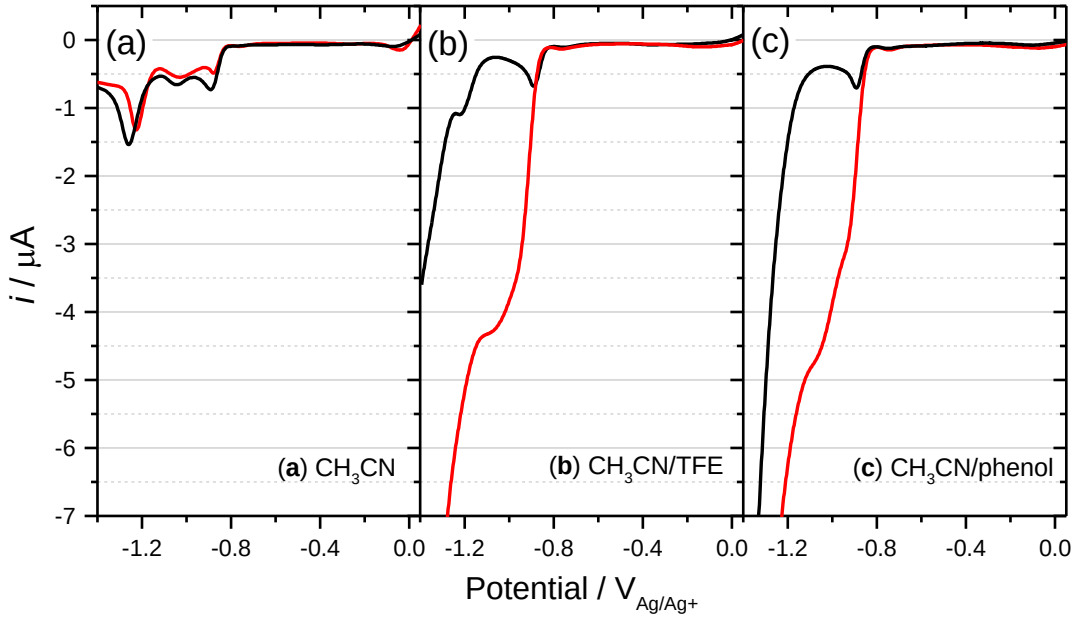

Figure 1. LSV's of $[Mn(bpy)(CO)_3Br]$ dissolved in CH_3CN recorded at 10 mV s^{-1} using an Au-Hg working electrode under Ar (black line) and CO_2 (red) sweeping from positive to negative potentials. Experiments were

performed in the absence of a Brønsted acid source (a) and in the presence of 1.5 M TFE (b) and 1.5 M phenol (c).

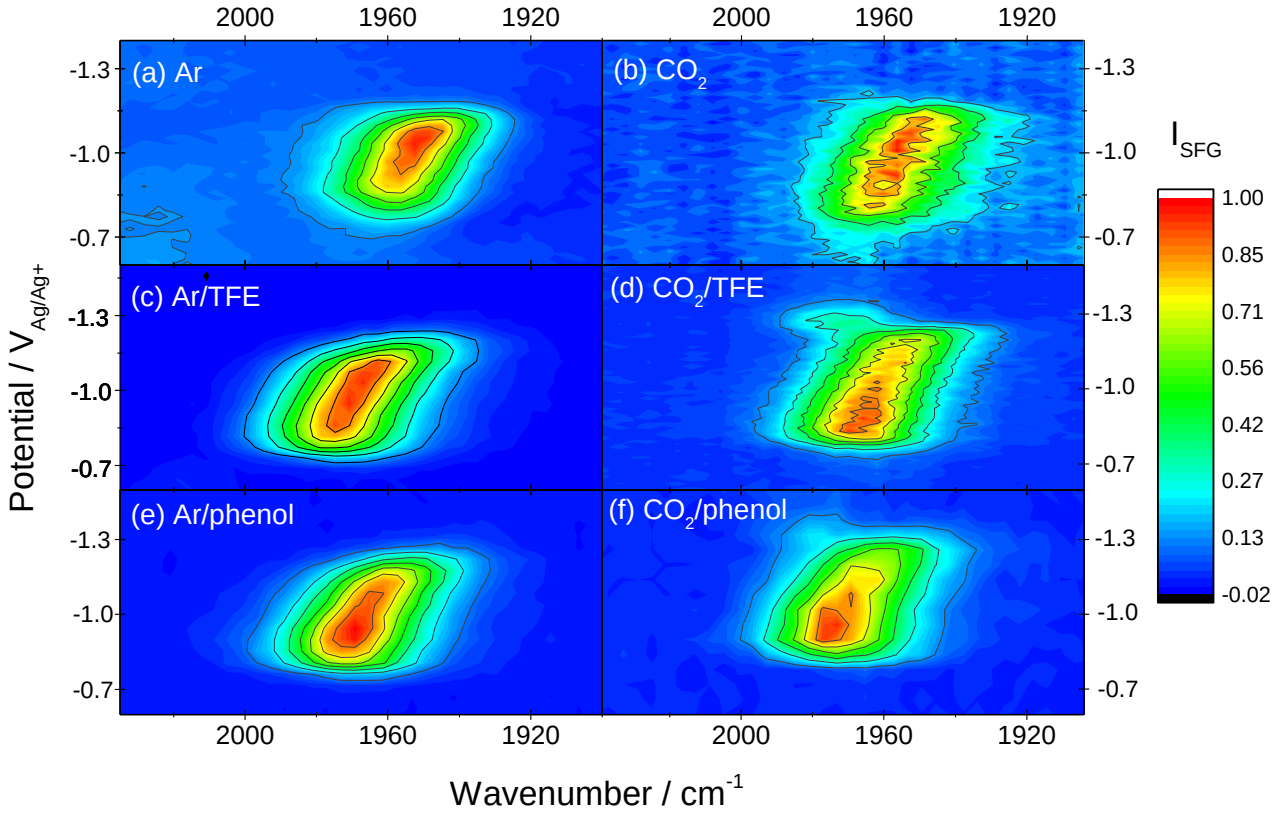

Figure 2. VSFG spectra recorded between -0.6 and -1.5 V during LSV's of $[Mn(bpy)(CO)_3Br]$ dissolved in CH_3CN, 20 mV s^{-1} (a), 10 mV s^{-1} (b-f) which are purged with either Ar (a, c, e) or CO_2 (b, d, f). In spectra (c,d) TFE is present, (e,f) phenol is present, both at 1.5 M. To suppress the non-resonant SFG response, spectra are recorded with a short (0.95 to 0.70 ps) delay between the broadband fs IR pulse (centre wavelength, 2005 cm^{-1}, full width half maximum 275 cm^{-1}, figure S4) and the fs-derived time-asymmetric ps 800 nm (visible) pulse.

B. In-situ resonant VSFG spectra

SEC-VSFG spectra recorded in the potential region (-0.7 to -1.3 V) where the dimer complex is present at a Au-Hg electrode are shown in figure 2 under a range of conditions. In all spectra the dominant strong ν(CO) band that occurs between *ca.* 1975 cm^{-1} and 1950 cm^{-1} can be assigned to $[Mn_2(bpy)_2(CO)_6]$ on the electrode surface. A full rational of the assignment of these VSFG spectra has been previously reported.[20] Briefly, it is made through a combination of analogy to reported ν(CO) spectra from past FTIR spectroelectrochemical studies[8] and the observation of the increase in intensity of ν(CO) VSFG band as those assignable to the starting

material $[Mn(bpy)(CO)_3X]^{n+}$ decrease, as the potential is swept negative (figure 3, S5-6). In Figure 2, (d) and (f) two additional bands are briefly present at *ca*. -1.3 V at approximately 1985 cm^{-1}, these have been discussed in a past publication and proposed to be ν(CO) bands of an intermediate species during the catalytic reduction of CO_2 by $[Mn(bpy)(CO)_3]^-$.[20]

On the basis of low temperature studies[7] it has been suggested that $[Mn_2(bpy)_2(CO)_6]$ could be formed following the rapid reaction of $[Mn(bpy)(CO)_3]^-$ with either $[Mn(bpy)(CO)_3Br]$ or $[Mn(bpy)(CO)_3(CH_3CN)]^+$ which would prevent a significant concentration of $[Mn(bpy)(CO)_3]^-$ from accumulating. Careful examination of the VSFG spectra for any weaker VSFG bands provided no indication of $[Mn(bpy)(CO)_3]^-$ formed *via* the surface stabilisation of $[Mn(bpy)(CO)_3]^\bullet$ at potentials positive of -1.2 V (blue pathway scheme 1), or the product of its interaction with H^+ $[Mn(bpy)(CO)_3H]$ (*ca.* 1991, 1892 and 1888(*sh*) cm^{-1})[20], figures S5-6. Instead only ν(CO) bands of $[Mn_2(bpy)_2(CO)_6]$ and $[Mn(bpy)(CO)_3(CH_3CN)]^+$ are observable in the re-scaled spectra, figures S5-6. The ν(CO) band of $[Mn(bpy)(CO)_3(CH_3CN)]^+$ is *ca.* 30 times weaker than those of $[Mn_2(bpy)_2(CO)_6]$ likely to be due to an additional resonance enhancement[6] given by the overlap between the wavelength of the "visible" laser (800 nm) and a UV-vis absorption feature of $[Mn_2(bpy)_2(CO)_6]$.

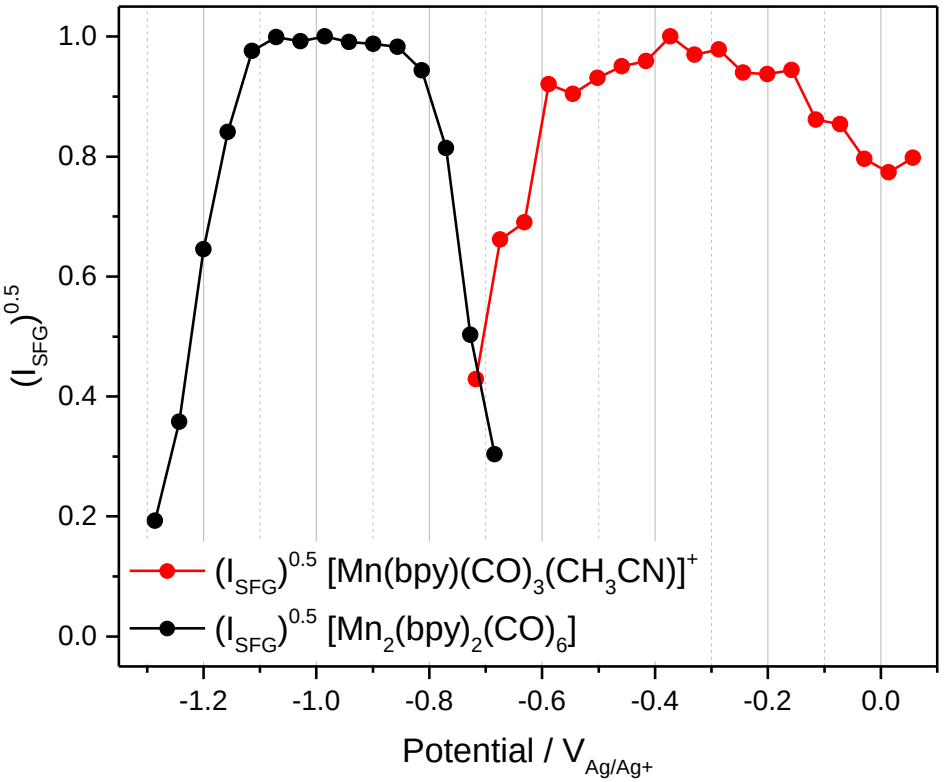

Figure 3. Square root of the areas of the main SEC-VSFG bands assigned to $[Mn(bpy)(CO)_3(CH_3CN)]^+$ (red) and $[Mn_2(bpy)_2(CO)_6]$ (black), under Ar in the presence of 1.5 M TFE, recorded during LSVs at 10 mV s^{-1}.

VSFG band intensities scale quadratically to the number density of the vibrational mode at the interface and also depend on the IR and Raman activities and strengths, and the orientation of the vibrational mode.[33] Consequently a plot of the square root of the amplitude of the VSFG modes of $[Mn_2(bpy)_2(CO)_6]$ and

$[Mn(bpy)(CO)_3(CH_3CN)]^+$ (figure 3) provide a reasonable descriptor, but not an absolute measure, of the concentration of these species at the electrode surface. Figure 3 shows that $[Mn(bpy)(CO)_3(CH_3CN)]^+$ from solution slowly accumulated either at, or on, the electrode surface as the potential was swept from +0.05 to -0.35 V. At potentials negative of -0.65 V the decrease in $[Mn(bpy)(CO)_3(CH_3CN)]^+$ correlates well with a rise in concentration of $[Mn_2(bpy)_2(CO)_6]$.

Despite the correlation between the loss of the VSFG bands assignable to $[Mn(bpy)(CO)_3(CH_3CN)]^+$ and the rise of the ν(CO) mode of $[Mn_2(bpy)_2(CO)_6]$, $[Mn_2(bpy)_2(CO)_6]$ accumulates at the electrode surface ~130 mV positive (-0.75 V) of the measured solution reduction potential (-0.88 V) of $[Mn(bpy)(CO)_3(CH_3CN/TFE)]^+$, figure 4. Inspection of the LSV shows that the growth of the VSFG band of $[Mn_2(bpy)_2(CO)_6]$ correlates with a small reductive feature occurring between -0.65 and -0.85 V, both under argon and CO_2 which is present in addition to the diffusion limited reduction of $[Mn(bpy)(CO)_3(CH_3CN)]^+$ at -0.88 V. It is therefore apparent that in our VSFG experiment we are monitoring either the adsorption (between +0.05 to -0.35 V) and subsequent reduction of $[Mn(bpy)(CO)_3(CH_3CN)]^+$, or the reduction and subsequent adsorption of $[Mn(bpy)_2(CO)_6]$ on the Au-Hg surface. Supporting these hypotheses are LSV's recorded on a Au electrode which shows a similar reductive features between -0.65 and -0.80 V (figure S7a), in contrast with GCE, a more inert electrode material, this reductive feature is not clearly observed (figure S7b). Therefore the majority of $[Mn_2(bpy)_2(CO)_6]$ formed between -0.85 and -0.95 V in the diffusion controlled process was not directly detected in the resonant VSFG spectra. Instead it is proposed that due to complete saturation of the electrode surface additionally formed $[Mn_2(bpy)_2(CO)_6]$ simply diffuses away from the electrode surface, see scheme in figure 4(b).

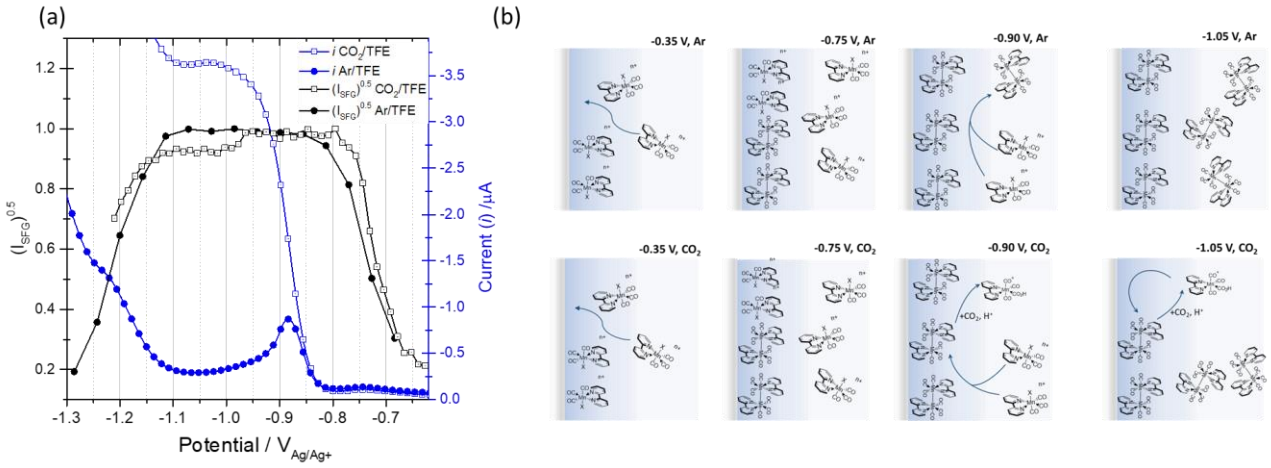

Figure 4. (a) *Blue:* LSV's of $[Mn(bpy)(CO)_3Br]$ dissolved in CH_3CN in the presence of 1.5 M TFE recorded at 10 mV s^{-1} using an Au-Hg working electrode under Ar (full circles) and CO_2 (empty squares) sweeping from positive to negative potentials; *Black:* square root of the area of the main band assigned to $[Mn_2(bpy)_2(CO)_6]$, under argon (full circles) and CO_2 (empty squares) recorded during the LSVs shown in blue. (b) Scheme depicting the surface behaviour at specified potentials under Ar and CO_2 in the presence of TFE.

Over the potential window of -0.7 to -1.2 V there is not a simple linear potential dependence of the frequency of the VSFG band of $[Mn_2(bpy)_2(CO)_6]$, figures 2 and 5. The frequency of an adsorbate vibrational mode is sensitive to factors such as (i) dipole-dipole coupling, where the modes are modified by resonant or partially resonant adsorbate dipole interactions,[34] (ii) changes in the adsorbate's environment, such as hydrogen bonding, solvation, coulombic repulsion and surface-adsorbate interacions[35,36] and (iii) changes in the external field (at the electrode interface) due to the modification of the applied potential to the electrode, commonly described as the Stark effect. Factors (i) and (ii) in particular are dependent on the orientation and surface coverage of the molecule. Disentangling the individual contributions to the observed potential dependence is complex, however it does offer a potentially rich source of information on the evolving surface and double layer structure. In our experiments we assume that no significant change in orientation of $[Mn_2(bpy)_2(CO)_6]$ at the surface (between -0.70 and -1.20 V (under Ar) and -0.70 and -0.95 V (under CO_2)) is occurring. Throughout the experiment one of the four ν(CO) mode dominates the VSFG spectra,[8] and no change in the relative intensities is observed, supporting this assumption. Instead we model the frequency shift of the ν(CO) peak with potential to a simplified 2-component model to disentangle the surface coverage and field-related Stark effects in the manner recently described by Pfisterer et al., in their study of sulfate absorption on Au using surface enhanced IR spectroscopy, Eq. 1.[35]

$$\nu_{CO_{(\phi,\Theta)}} = \mathrm{K}_{\phi}(\phi - \phi_0) + \mathrm{K}_{\Theta}\Theta + \upsilon_0 \qquad \text{Eq. 1}$$

Where ϕ refers to the applied potential, K_{ϕ} the Stark tuning constant, $\Theta(\phi)$ the coverage at an applied potential, K_{Θ} the coverage tuning constant, and ν_0 the vibrational mode frequency at the potential of initial adsorption. Full details of the fitting procedure can be found in the electronic supporting information (Figures S8-9 and related text). Briefly by using the square root of the intensity of the VSFG as relative descriptor of surface coverage, and by assuming that potential ranges of constant VSFG intensity correspond to constant surface coverage/orientation we are able to reproduce the experimentally observed potential dependence trend of the ν(CO) mode of $[Mn_2(bpy)_2(CO)_6]$, figure 5. Under Ar we can examine the full potential range over which the complex can be detected by VSFG (-0.7 to -1.2 V, figure 5b, solid line) and we find that $\mathrm{K}_{\phi} = 45 \pm 7$ cm^{-1}/V and $\mathrm{K}_{\Theta} = 10 \pm 3$ cm^{-1}/Θ. At potentials negative of -0.95 V under CO_2 the onset of catalysis is expected to lead to the presence of a complex mixture of surface species making it only possible to apply the model to a smaller voltage window, nonetheless similar tuning rates ($\mathrm{K}_{\phi} = 31 \pm 3$ cm^{-1}/V and $\mathrm{K}_{\Theta} = 12 \pm 2$ cm^{-1}/Θ) are found and good fit to the experimental data is achieved (figure 5c).

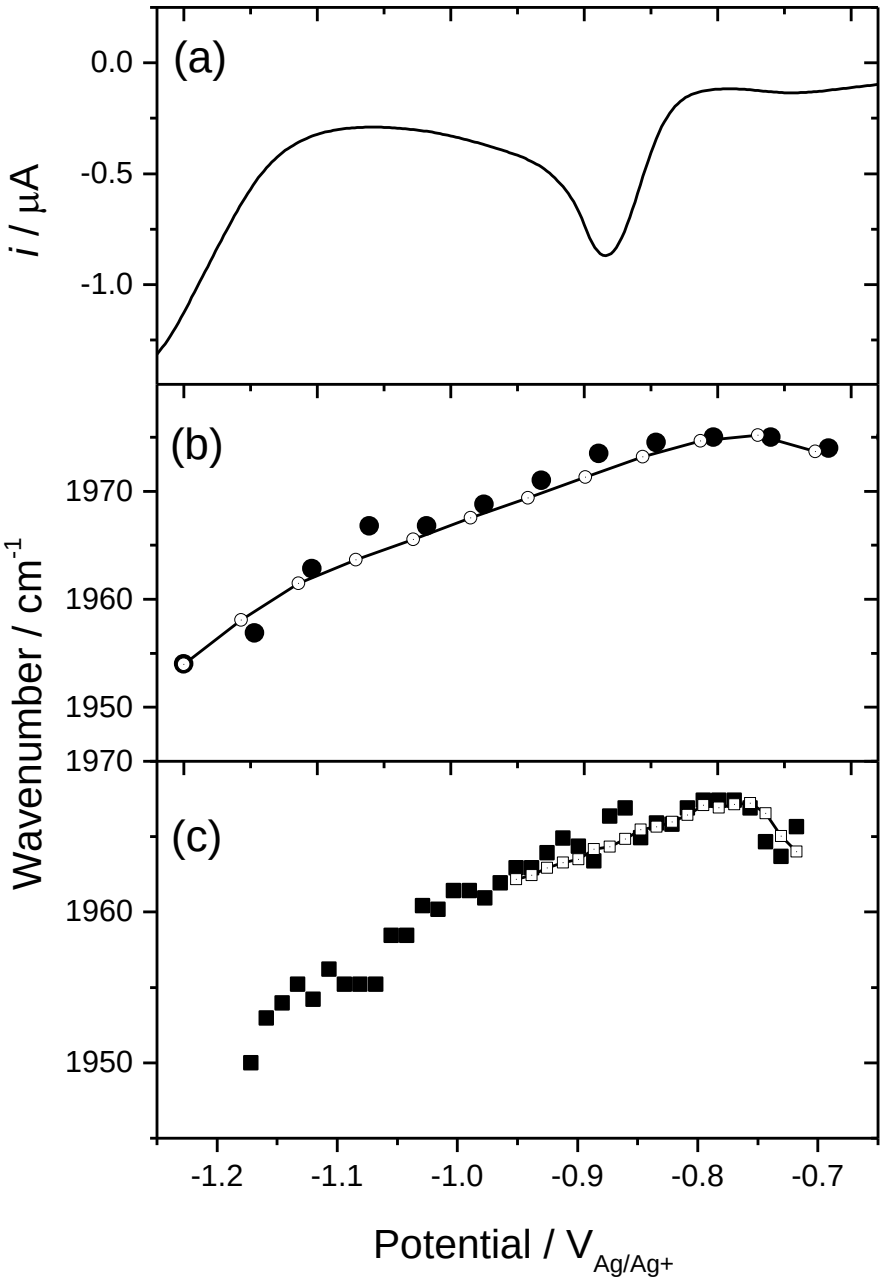

Figure 5. (a) LSVs of of [Mn(bpy)(CO)$_3$Br] dissolved in CH_3CN in the presence of 1.5 M TFE recorded at 10 mV s^{-1} using a Au-Hg working electrode under Ar; (b,c) peak centres of the VSFG mode of [Mn_2(bpy)$_2$(CO)$_6$] measured during the SEC experiment under Ar and CO_2 respectively. Open circle/squares with solid line (b, c) are the result of fitting to the surface coverage model described above.

We now turn to the proposed mechanism of CO_2 catalysis following the direct interaction of [Mn_2(bpy)$_2$(CO)$_6$] with CO_2 and H^+. During VSFG experiments in the absence of CO_2 but presence of an acid, or under CO_2 without an acid source, we find that the I_{SFG} of [Mn_2(bpy)$_2$(CO)$_6$] is approximately constant between -0.85 and -1.10 V (figure 2 a,b,c,e). In contrast under CO_2 in the presence of H^+ (figure 2 d,f) we note a marked decrease in the amplitude of the SFG band of [Mn_2(bpy)$_2$(CO)$_6$] between -0.95 and -1.10 V. The decrease in amplitude of the VSFG band of [Mn_2(bpy)$_2$(CO)$_6$] at the electrode surface in the presence of CO_2 and H^+ is in-line with

the proposed "dimer" mechanism of CO_2 reduction by Deronzier et al., (red pathway scheme 1) which occurs without the need for the direct generation of $[Mn(bpy)(CO)_3]^-$ and figure 4 shows a remarkable inverse correlation between the VSFG band amplitude and the catalytic current from this lower overpotential pathway.[37]

Figure 4 also shows that the decrease in the amplitude of the $[Mn(bpy)_2(CO)_6]$ band is not immediate following formation of this complex under CO_2 in the presence of an acid source. EPR studies by Deronzier *et al.*, have shown the formation of a *mer* Mn^{II}-CO_2H complex following the interaction of CO_2 and H^+ and $[Mn_2(Me\text{-}bpy)_2(CO)_6]$. The unchanged surface concentration of $[Mn_2(bpy)_2(CO)_6]$ under CO_2/TFE between -0.85 and -0.95 V prior to a decay in $I_{SFG}{}^{0.5}$ of 8% by -1.0 V can be explained by the rapid replenishment of any surface $[Mn_2(bpy)_2(CO)_6]$ that initially reacts with CO_2/H^+. At potentials positive of -0.95 V our LSV shows that a significant concentration of $[Mn(bpy)(CO)_3(CH_3CN)]^+$ remains within the diffusion layer, figure 1. At potentials negative of -0.95 V the LSV shows that catalysis onsets and the rate of consumption of $[Mn_2(bpy)_2(CO)_6]$ then exceeds the rate of its replenishment by the reduction of any $[Mn(bpy)(CO)_3(CH_3CN)]^{n+}$ that diffuses towards the electrode surface, figure 4b, bottom part. To date, direct observation of the initially formed surface CO_2 adduct has been unsuccessful which may indicate either that the equilibrium constant for the reaction of $[Mn_2(bpy)_2(CO)_6]$ with CO_2/H^+ is small or that any CO_2 reduction intermediates in this mechanism do not form ordered structures at/close to the electrode surface.

DISCUSSION

VSFG spectroscopy has been shown to be able to detect the formation and behaviour of a surface population of $[Mn_2(bpy)_2(CO)_6]$ under both Ar and CO_2 at potentials significantly positive (130 mV) of the expected reduction potential for the related solution species. Although we are unable to rule out that the mechanism of formation of this surface population is *via* the initial generation of $[Mn(bpy)(CO)_3]^-$ through surface stabilisation of $[Mn(bpy)(CO)_3]^\bullet$ at the metal electrodes used (blue pathway, scheme 1), it is notable that we were unable to detect either $[Mn(bpy)(CO)_3]^-$ or $[Mn(bpy)(CO)_3H]$ in our experiments, even though the instrument S/N was sufficient for detecting the parent complex. Instead we propose it is most likely that the surface population of $[Mn_2(bpy)_2(CO)_6]$ forms following the reduction of adsorbed $[Mn(bpy)(CO)_3(CH_3CN)]^+$ to yield $[Mn(bpy)(CO)_3]^\bullet$ which then dimerises. The proposed reduction of $[Mn(bpy)(CO)_3(CH_3CN)]^+$ to $[Mn_2(bpy)_2(CO)_6]$ on the electrode surface (figure 3) is in-line with the known mechanism of dimer formation *via* rapid dimerisation of $[Mn(bpy)(CO)_3]^\bullet$ that occurs in solution.[22]

Of significance is the large catalytic current between -0.9 and -1.1 V in the presence of CO_2 and a suitable acid source. Although the presence of a low overpotential pathway has been shown numerous times with related complexes with modified bipyridine ligands and in surface immobilised systems,[5,14,23,24] early reports on the prototypical complex used using a GCE and water (5%) as the proton source did not report catalytic currents due to this mechanism.[6] Electrochemical studies using a range of electrode materials here show that the nature of the electrode material is not critical for catalysis to occur *via* the lower overpotential pathway, instead we

find that nature of the acid is. The lack of sensitivity to electrode material supports the previously proposed dimer mechanism of Deronzier et al., with direct CO_2/H^+ interacting directly with $[Mn_2(bpy)_2(CO)_6]$ and it appears to rule out the alternative pathway (blue) in scheme 1. pKa's in acetonitrile for the acids considered have been reported (TFE (26.4), phenol (21.6) and water/CO_2 (26.6))[12] and it is clear that pKa alone cannot account for the differing behaviour in water and TFE/phenol. It has been calculated that the binding of CO_2 to $[Mn(bpy)(CO)_3]^-$ in the presence of TFE is enabled by both the initial stabilisation of the CO_2 adduct through hydrogen bonding to TFE molecules and by the subsequent exergonic carbonation of the TFE^-/ TFEH homoconjugate[13] and it seems likely that similar specific interactions are required to enable CO_2 insertion into the dimer complex.

Although we do not directly observe intermediates for the dimer pathway, the observation that $[Mn_2(bpy)_2(CO)_6]$ can be formed at the electrode 130 mV positive of the onset of catalysis via the dimer pathway does provide some insight into the mechanisms of CO_2 reduction. Past UV-vis-SEC studies on a related Mn complex with methyl substituents on the bpy ligand ($[Mn(Me_2\text{-}bpy)(CO)_3Br]$)[21] showed that under Ar the dimer complex $[Mn_2(Me_2\text{-}bpy)_2(CO)_6]$ was relatively stable once formed. Introduction of CO_2 lead to a rapid loss of the UV-vis spectral features of the dimer, indicating rapid reaction to form a CO_2 adduct, identified as $[mer\text{-}Mn(Me_2\text{-}bpy)(CO)_3(CO_2H)]^+$ even in the absence of an applied potential. Here, we carried out similar experiments using $[Mn(bpy)(CO)_3Br]$ in CH_3CN with TFE, figure S8. These showed that under electrolysis conditions (-1.05 V) in the presence of CO_2 the concentration of the dimer that can be achieved is only ~60% of what was found under argon, in-line with similar observations by Deronzier on $[Mn(Me_2\text{-}bpy)(CO)_3Br]$.[21] The lower steady state-concentration of $[Mn_2(bpy)_2(CO)_6]$ confirms that the complex is being consumed during the catalytic cycle. Significantly, in figure S8 when the potential control was removed the CO_2-purged solution showed a very rapid loss of the UV-Vis bands assigned to $[Mn_2(bpy)_2(CO)_6]$. In contrast the UV-Vis bands of $[Mn_2(bpy)_2(CO)_6]$ only decayed slowly in argon-purged CH_3CN/TFE solutions. These results indicate rapid reaction of CO_2 with the dimer at the potentials applied during the experiment (-1.05 $V_{Ag/Ag+}$) when in the presence of TFE, and that CO_2, in the presence of a suitable acid source, can interact with any $[Mn_2(bpy)_2(CO)_6]$ present even in the absence of an applied potential.

Despite the fact that CO_2 adducts will be able to form as soon as $[Mn_2(bpy)_2(CO)_6]$ is generated (negative of -0.7 V), it is notable that catalysis does not onset until potentials negative of -0.95 V, providing a value for the reduction potential of the electrochemical limiting step. On the basis of past EPR studies it is likely that the initially formed adduct is $[mer\text{-}Mn(bpy)(CO)_3(CO_2H)]^+$. Deronzier et al. proposed a one electron reduction and protonation of this species, followed by CO and H_2O loss to reform $[Mn(bpy)(CO)_3(CH_3CN)]^+$ (scheme 2)[21]. Grills et al. have suggested that reduction to form $[mer\text{-}Mn(bpy)(CO)_3(CO_2H)]$ is more likely to occur and that subsequent protonation to form $[Mn(bpy)(CO)_4]^+$ can take place.[15] Although the exact reduction potential of $[Mn(bpy)(CO)_4]^+$ to expel CO and reform the dimer complex is unknown we did recently detect an intermediate at the electrode surface formed following the interaction with $[Mn(bpy)(CO)_3]^-$ with CO_2 in strong acids.[20] Through the noted dependence on acid strength and isotopic labelling studies we were able to identify the intermediate to be either $[Mn(bpy)(CO)_4]^+$ or $[Mn(bpy)(CO)_4]$ formed during protonation first

catalysis, with DFT calculations allowing us to conclude that on the balance of probability the complex was $[Mn(bpy)(CO)_4]^+$. Significantly this complex was found to be stable at potentials between -1.2 and -1.1 V, considerably negative of the onset of catalysis by the dimer pathway. It is therefore apparent that the nature of the limiting electron transfer process remains unknown and that further, likely theory studies, will be required to identify this species. Indeed the mechanism of catalysis following the formation of [*mer*-$Mn(bpy)(CO)_3(CO_2H)$] may be even more complex that the two pathways previously proposed[15,21] and we suggest that at this point a third pathway should not be discounted – the reduction of [*mer*-$Mn(bpy)(CO)_3(CO_2H)$] prior to protonation, in a mechanism analogous to the reduction first pathway that is known to occur following the formation of $[Mn(bpy)(CO)_3(CO_2H)]$, scheme 2. Although $[Mn(bpy)(CO)_3(CO_2H)]$ is not reduced until significantly more negative potentials (*ca.* -1.69 V (SCE[13] *ca.* -1.49 V versus the Ag pseudo reference electrode used here) the role of the differing coordination geometry in determining the electrochemical stability requires further investigation.

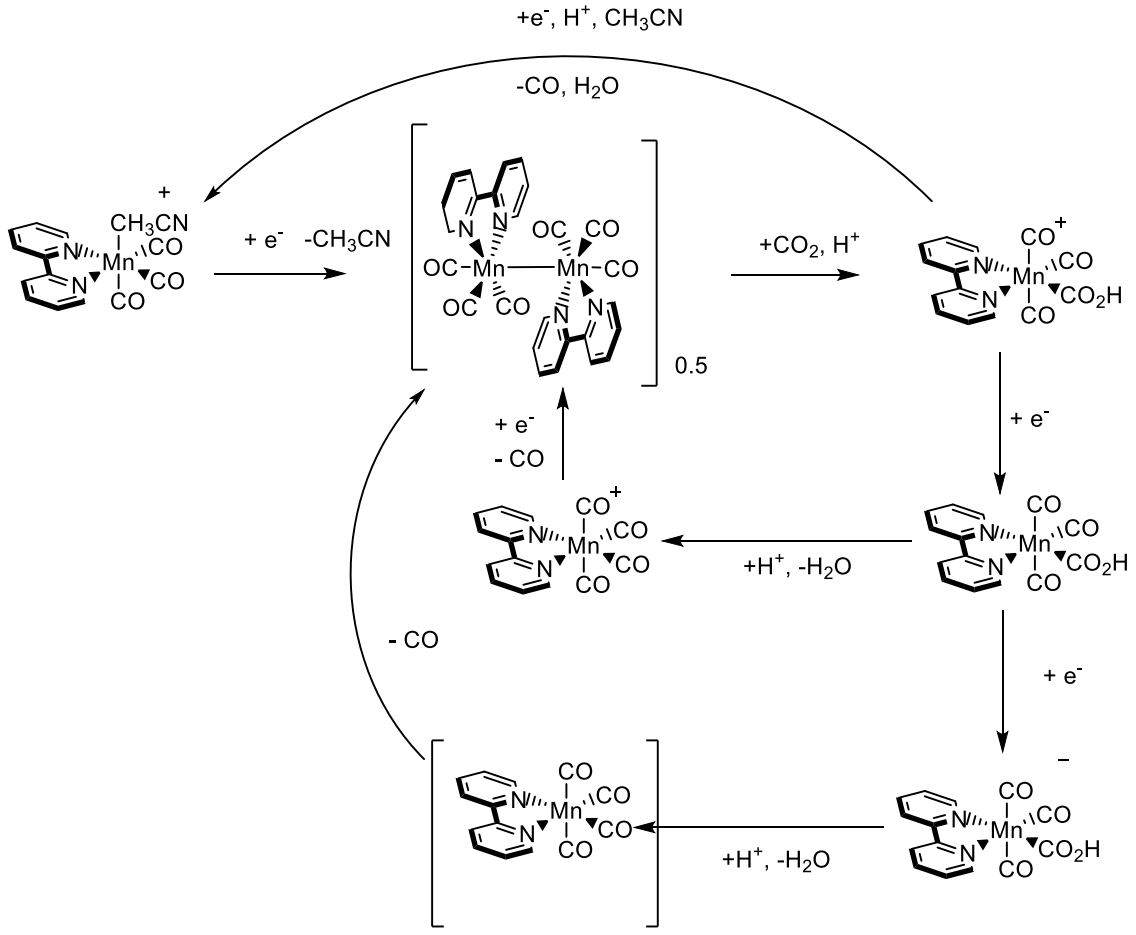

Scheme 2: Potential mechanisms of carbon dioxide reduction following the interaction of $[Mn_2(bpy)_2(CO)_6]$ with CO_2 in the presence of a suitable acid. Three possible mechanisms are proposed, with direct reduction and protonation leading to CO and water loss[21] (top), protonation first[14] (middle) and reduction first of [*mer*-$Mn(bpy)(CO)_3(CO_2H)$].

CONCLUSIONS

In-situ VSFG spectroscopy has been used to investigate the formation and behaviour of surface adsorbed $[Mn_2(bpy)_2(CO)_6]$ at a Au-Hg electrode during LSV measurements. Significantly our measurements provide insight into a low-overpotential catalytic pathway which occurs following the interaction of CO_2 and $[Mn_2(bpy)_2(CO)_6]$ in the presence of a suitable acid. Although past studies have reported such behaviour using complexes with modified bipyridine ligands to the best of our knowledge such behaviour has not been highlighted with $[Mn_2(bpy)_2(CO)_6]$. Finally detailed analysis of the VSFG data, including analysis of the potential dependence of the peak maxima of a key ν(CO) mode, provides important insights into the fundamental behaviour of $[Mn_2(bpy)_2(CO)_6]$ at the electrode surface. These VSFG studies further highlight the capability of the technique to provide a high level of detail on the molecular interactions occurring at electrified interfaces under working conditions which is of significance to the wider electrochemistry community.

CONFLICTS OF INTEREST

There are no conflicts to declare

ACKNOWLEDGEMENTS

We are grateful to C. Smith (University of Liverpool) for the synthesis of 1. This work was carried out at the Ultra facility of the UK Central Laser Facility during experiments 15130005, 16130016 and 16230052. A.J.C. and G.N. acknowledge support from EPSRC (EP/K006851/1, EP/P034497/1 and EP/N010531/).

REFERENCES

1. A. J. Cowan and J. R. Durrant, *Chem. Soc. Rev.*, 2013, **42**, 2281–93.
2. J. J. Walsh, G. Neri, C. L. Smith, and A. J. Cowan, *Organometallics*, 2018.
3. A. Tatin, C. Comminges, B. Kokoh, C. Costentin, M. Robert, and J.-M. Savéant, *Proc. Natl. Acad. Sci.*, 2016, **113**, 5526–5529.
4. C. Costentin, M. Robert, J.-M. Savéant, and A. Tatin, *Proc. Natl. Acad. Sci.*, 2015, **112**, 6882–6886.
5. J. J. Walsh, G. Neri, C. L. Smith, and A. J. Cowan, *Chem. Commun.*, 2014, **50**, 12698–12701.
6. M. Bourrez, F. Molton, S. Chardon-Noblat, and A. Deronzier, *Angew. Chemie Int. Ed.*, 2011, **50**, 9903–9906.
7. B. D. Rossenaar, F. Hartl, D. J. Stufkens, C. Amatore, E. Maisonhaute, and J.-N. Verpeaux, *Organometallics*, 1997, **16**, 4675–4685.
8. F. Hartl, B. D. Rossenaar, G. J. Stor, and D. J. Stufkens, *Recl. Trav. Chim. Pays-Bas*, 1995, **114**, 565-.

9. F. Hartl, P. Rosa, L. Ricard, P. Le Floch, and S. Záliš, *Coord. Chem. Rev.*, 2007, 251, 557–576.

10. N. Elgrishi, M. B. Chambers, X. Wang, and M. Fontecave, *Chem. Soc. Rev.*, 2017, **46**, 761–796.

11. C. Riplinger, M. D. Sampson, A. M. Ritzmann, C. P. Kubiak, and E. A. Carter, *J. Am. Chem. Soc.*, 2014, **136**, 16285–16298.

12. C. Riplinger and E. A. Carter, *ACS Catal.*, 2015, **5**, 900–908.

13. Y. C. Lam, R. J. Nielsen, H. B. Gray, and W. A. Goddard, *ACS Catal.*, 2015, **5**, 2521–2528.

14. D. C. Grills, M. Z. Ertem, M. McKinnon, K. T. Ngo, and J. Rochford, *Coord. Chem. Rev.*, 2018, **374**, 173–217.

15. M. Stanbury, J.-D. Compain, and S. Chardon-Noblat, *Coord. Chem. Rev.*, 2018, **361**, 120–137.

16. D. C. Grills, J. A. Farrington, B. H. Layne, S. V. Lymar, B. A. Mello, J. M. Preses, and J. F. Wishart, *J. Am. Chem. Soc.*, 2014, **136**, 5563–5566.

17. M. L. Clark, A. Ge, P. E. Videla, B. Rudshteyn, C. J. Miller, J. Song, V. S. Batista, T. Lian, and C. P. Kubiak, *J. Am. Chem. Soc.*, 2018.

18. K. T. Ngo, M. McKinnon, B. Mahanti, R. Narayanan, D. C. Grills, M. Z. Ertem, and J. Rochford, *J. Am. Chem. Soc.*, 2017, **139**, 2604–2618.

19. M. D. Sampson, A. D. Nguyen, K. A. Grice, C. E. Moore, A. L. Rheingold, and C. P. Kubiak, *J. Am. Chem. Soc.*, 2014, **136**, 5460–5471.

20. G. Neri, J. J. Walsh, G. Teobaldi, P. M. Donaldson, and A. J. Cowan, *Nat. Catal.*, 2018.

21. M. Bourrez, M. Orio, F. Molton, H. Vezin, C. Duboc, A. Deronzier, and S. Chardon-Noblat, *Angew. Chemie - Int. Ed.*, 2014, **53**, 240–243.

22. D. C. Grills, J. A. Farrington, B. H. Layne, S. V. Lymar, B. A. Mello, J. M. Preses, and J. F. Wishart, *J. Am. Chem. Soc.*, 2014, **136**, 5563–5566.

23. B. Reuillard, K. H. Ly, T. E. Rosser, M. F. Kuehnel, I. Zebger, and E. Reisner, .

24. J. J. Walsh, M. Forster, C. Smith, G. Neri, R. Potter, and A. J. Cowan, *Phys. Chem. Chem. Phys.*, 2018, **20**, 6811–6816.

25. K. T. Ngo, M. McKinnon, B. Mahanti, R. Narayanan, D. C. Grills, M. Z. Ertem, and J. Rochford, *J. Am. Chem. Soc.*, 2017, **139**, 2604–2618.

26. B. A. Rosen, J. L. Haan, P. Mukherjee, B. Braunschweig, W. Zhu, A. Salehi-Khojin, D. D. Dlott, and R. I. Masel, *J. Phys. Chem. C*, 2012, **116**, 15307–15312.

27. N. García Rey and D. D. Dlott, *J. Phys. Chem. C*, 2015, **119**, 20892–20899.

28. R. B. Kutz, B. Braunschweig, P. Mukherjee, D. D. Dlott, and A. Wieckowski, *J. Phys. Chem. Lett.*, 2011, **2**, 2236–2240.

29. G. Neri, P. M. Donaldson, and A. J. Cowan, *J. Am. Chem. Soc.*, 2017, **139**, 13791–13797.

30. J. He, N. J. J. Johnson, A. Huang, and C. P. Berlinguette, *ChemSusChem*, 2018, **11**, 48–57.

31. G. J. Stor, S. L. Morrison, D. J. Stufkens, and A. Oskam, *Organometallics*, 1994, **13**, 2641–2650.

32. T. E. Rosser, C. D. Windle, and E. Reisner, *Angew. Chemie Int. Ed.*, 2016, **55**, 7388–7392.

33. A. G. Lambert, P. B. Davies, and D. J. Neivandt, *Appl. Spectrosc. Rev.*, 2005, 40, 103–145.

34. R. M. M. Hammaker, S. A. a Francis, and R. P. P. Eischens, *Spectrochim. Acta*, 1965, **21**, 1295–1309.

35. J. H. K. Pfisterer, U. E. Zhumaev, W. Cheuquepan, J. M. Feliu, and K. F. Domke, *J. Chem. Phys.*, 2019, **150**, 41709.

36. P. Zhang, Y. Wei, J. Cai, Y.-X. Chen, and Z.-Q. Tian, *Chinese J. Catal.*, 2016, **37**, 1156–1165.

37. M. Bourrez, M. Orio, F. Molton, H. Vezin, C. Duboc, A. Deronzier, and S. Chardon-Noblat, *Angew. Chemie Int. Ed.*, 2014, **53**, 240–243.